SNR Measurement of Superregenerative Oscillators

Jordi Bonet-Dalmau, Pere Palà-Schönwälder, F. Xavier Moncunill-Geniz
Department of Mining, Industrial and ICT Engineering (EMIT), Manresa School of Engineering (EPSEM),
Universitat Politècnica de Catalunya (UPC), 08242 Manresa, Spain
jordi.bonet@upc.edu

***Abstract*—In this paper a method to measure the signal-to-noise ratio of superregenerative oscillators is presented. A spectrum analyzer can easily be coupled to a superregenerative oscillator without paying attention to possible loading effects. With just two measurements of the displayed power spectrum, in combination with the resolution bandwidth of the spectrum analyzer and the quench frequency of the oscillator, the signal-to-noise ratio is determined in a straightforward way. This is supported analytically with results from a frequency-domain analysis technique. Examples of the power displayed by a spectrum analyzer are given to provide insight into the explained procedure.**

***Index Terms*—Superregenerative oscillator, noise, SNR, frequency domain analysis, wireless receiver.**

I. Introduction

INTRODUCED almost a century ago [1], superregenerative (SR) receivers are still an active topic of interest as a low-power and low-complexity receiver. Both features are becoming even more and more relevant in the current context of the IoT paradigm and its applications to fields such as Industry 4.0 and Smart Cities, among many other areas where cost and power consumption are a major driving force allowing to ignore some of the shortcomings of the SR alternative.

Nowadays, the SR receiver is able to detect almost any type of modulation, ranging from narrow-band analog and digital modulations (AM, FM [2], [3], and PM [4], [5]) to ultra-wide band modulations (AM [6] and FM [7]), with applications ranging from the IoT field [8], [9] to base-band amplification [10] or to ultrasound wake-up receivers [11].

Noise analysis is a very relevant issue in RF receivers and some results on the signal-to-noise ratio (SNR) of SR circuits were already presented in [2]. Further results have been given lately in [12]–[16]. In this paper, we build on a method to quantify noise in SR receivers [17] which is, in turn, based on the frequency domain analysis technique [18], to experimentally compute SNR of an SR receiver.

II. Computing the Power Spectrum Displayed by a Spectrum Analyzer

An SR receiver can be modeled by the block diagram in Fig. 1, where the part labeled SRO represents the core of the receiver, the SR oscillator. The response to a sinusoidal input signal $v_i(t)$ of frequency ω_{in} and a periodic (not necessarily sinusoidal [19]) quench signal $k_a(t)$ of frequency ω_q is a combination of sinusoids, each one of frequency $\omega_{in} + k\omega_q$, with k integer [18].

Work co-financed by the European Regional Development Fund of the European Union in the framework of the ERDF Operational Program of Catalonia 2014-2020 by the grant 001-P-001643 - Looming Factory.

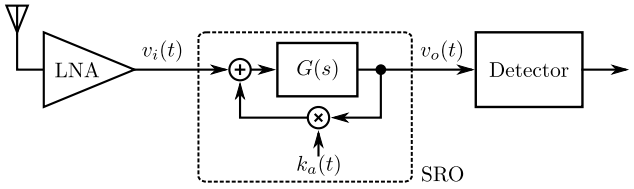

Fig. 1. Block diagram of the SR receiver.

By using superposition, this technique can also be applied when the input is a combination of sinusoids and, as is explained in [17], to a continuous input spectrum such as that of white noise.

In [17] a method to compute signal and noise power spectra in SRO was presented. Based on this method, we are going to show an experimental method to determine the SNR of an SRO based on the observation of the information given by a spectrum analyzer (SA).

The power displayed by a swept-tuned SA at a given frequency ω_c is the power at the output of a narrow band-pass filter (which sets the resolution bandwidth, RBW) whose input is a down-converted portion of the input signal spectrum around the center frequency ω_c, to the center frequency ω_{bp} of this band-pass filter. The Gaussian band-pass filters commonly available on most SAs exhibits the frequency response

$$|H_{SA}(\omega, \omega_{bp})| = e^{-\frac{\left(\frac{\omega-\omega_{bp}}{2\pi}\right)^2}{2\sigma^2}}. \tag{1}$$

The parameter σ, in Hz, of the band-pass is related to the SA RBW adjustment, given also in Hz. This figure is sometimes defined as the $3\,\mathrm{dB}$ bandwidth ($\mathrm{BW_{3dB}}$) and sometimes as the equivalent noise bandwidth (ENBW) of the SA band-pass filter. These figures are related as

$$\mathrm{BW_{3dB}} = \sigma 2\sqrt{\ln 2}, \tag{2}$$

$$\mathrm{ENBW} = \sigma\sqrt{\pi}. \tag{3}$$

The signal spectrum at the output of the SRO for a sinusoidal input of frequency ω_0, the center frequency of the selective network $G(s)$ in Fig. 1, has the form

$$C_{\text{signal}}(\omega) = \sum_{n=-n_1}^{n=n_2} C_n \delta(\omega - (\omega_0 + n\omega_q)), \tag{4}$$

where C_n is the amplitude of the impulse at frequency

$$\omega_{0,n} = \omega_0 + n\omega_q. \tag{5}$$

So, the total SRO signal output power taking into account both sides of the spectrum is given by [17]

$$P_{\text{signal}} = 2\sum_{n=-n_1}^{n=n_2} |C_n|^2. \tag{6}$$

Each of the impulses of the signal spectrum gives an SA power response with the shape of the frequency response (1) squared, centered at $\omega_c = \omega_{0,n}$, and amplitude given by

$$P_{\text{signal SA}}(\omega_{0,n}) = 2\,|C_n|^2. \tag{7}$$

Now, let us consider noise. The double-sided noise power spectral density (PSD) at the output of the SRO in the interval $\omega_{i'} - \Delta\omega/2 \leq \omega < \omega_{i'} + \Delta\omega/2$ is constant and equal to

$$\text{PSD}(\omega_{i'}) = |C_{i'}|^2 \frac{2\pi}{\Delta\omega}, \tag{8}$$

where $|C_{i'}|^2$ is measured in V^2 and PSD in V^2/Hz. This PSD is obtained after distributing the power of each one of the following impulses over the bandwidth $\Delta\omega$ around its frequency $\omega_{i'}$:

$$C_{\text{noise}}(\omega) = \sum_{i'=-K_1}^{i'=K_2} C_{i'}\delta(\omega - \omega_{i'}). \tag{9}$$

with

$$\omega_{i'} = \omega_0 + i'\Delta\omega, \tag{10}$$

and $\Delta\omega = \omega_q/m$ sufficiently small, which is achieved with a sufficiently high value of m. The total SRO noise output power taking into account both sides of the spectrum is given by

$$P_{\text{noise}} = 2\sum_{i'=-K_1}^{i'=K_2} |C_{i'}|^2. \tag{11}$$

Each one of the noise intervals centered at $\omega_{i'}$ with constant PSD given by (8) gives an SA power that is two times the power contained in an interval equal to the ENBW (3) of the SA band-pass filter (1), i.e.

$$P_{\text{noise SA}}(\omega_{i'}) = 2\text{PSD}(\omega_{i'})\text{ENBW}. \tag{12}$$

This last expression considers that the ENBW is small compared with the variation of the noise PSD with the frequency, assumption that can be assured changing the RBW adjustment of the SA.

III. SNR Measurement

As was shown in [17], the SNR at the output of the SRO can be computed in a straightforward way from (11) and (6):

$$\text{SNR} = \frac{P_{\text{signal}}}{P_{\text{noise}}} = \frac{\sum_{n=-n_1}^{n=n_2} |C_n|^2}{\sum_{i'=-K_1}^{i'=K_2} |C_{i'}|^2}. \tag{13}$$

The next step is to experimentally determine the SNR from the information displayed by the SA. A first idea is to compute the SNR in the interval $\omega_0 - \omega_q/2 \leq \omega < \omega_0 + \omega_q/2$, called

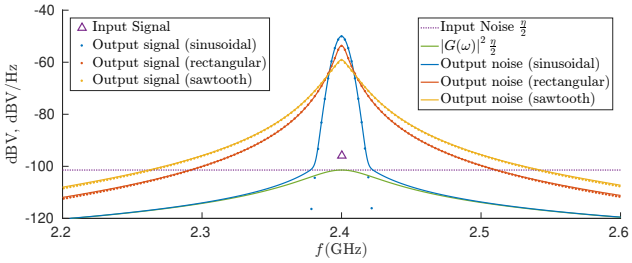

Fig. 2. PSD of noise in dBV/Hz and signal power spectrum in dBV at the output of the SRO for each of the quench signals $k_a(t)$ in Fig. 3. For each quench signal, the PSD of noise has been scaled to make its maximum value in dBV/Hz equal to the maximum value of the signal power spectrum in dBV.

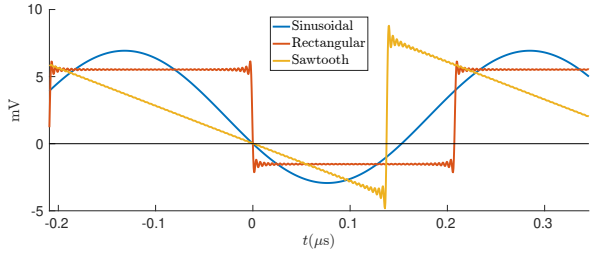

Fig. 3. Instantaneous damping factor $\xi(t)$ for sinusoidal, rectangular and sawtooth quench signals $k_a(t)$. $\xi(t) = \frac{1-k_0k_a(t)}{2Q_0}$.

$\Delta\omega_{0,0}$. Following the reasoning made in the previous section, the signal power contained in all this interval is

$$P_{\text{signal}}(\Delta\omega_{0,0}) = 2\,|C_0|^2, \tag{14}$$

and the noise power contained in the same interval is

$$P_{\text{noise}}(\Delta\omega_{0,0}) = 2\text{PSD}(\omega_{i'})f_q, \tag{15}$$

with $f_q = \frac{\omega_q}{2\pi}$. So, the SNR in this interval using (14) and (15) is

$$\text{SNR}(\Delta\omega_{0,0}) = \frac{P_{\text{signal}}(\Delta\omega_{0,0})}{P_{\text{noise}}(\Delta\omega_{0,0})} = \frac{2\,|C_0|^2}{2\text{PSD}(\omega_{0,0})f_q}. \tag{16}$$

This expression can be related to the values given by the SA using (7) and (12) as

$$\text{SNR}(\Delta\omega_{0,0}) = \frac{P_{\text{signal SA}}(\omega_{0,0})}{P_{\text{noise SA}}(\omega_{0,0})}\frac{\text{ENBW}}{f_q}. \tag{17}$$

We could repeat the computation of SNR in other intervals $\omega_0 + n\omega_q - \omega_q/2 \leq \omega < \omega_0 + n\omega_q + \omega_q/2$, called $\Delta\omega_{0,n}$. In each one of these intervals the SNR is

$$\text{SNR}(\Delta\omega_{0,n}) = \frac{P_{\text{signal SA}}(\omega_{0,n})}{P_{\text{noise SA}}(\omega_{0,n})}\frac{\text{ENBW}}{f_q}. \tag{18}$$

The addition of all the noise and signal power will give the overall SNR as

$$\text{SNR}_{\text{SA}} = \frac{\sum_{n=-n_1}^{n=n2} P_{\text{signal SA}}(\omega_{0,n})}{\sum_{n=-n_1}^{n=n2} P_{\text{noise SA}}(\omega_{0,n})}\frac{\text{ENBW}}{f_q}. \tag{19}$$

As can be seen in Fig. 2 (extracted from [17]), the shape of the envelope of the PSD of noise and of the signal power spectrum is almost the same. For the purpose of computing power,

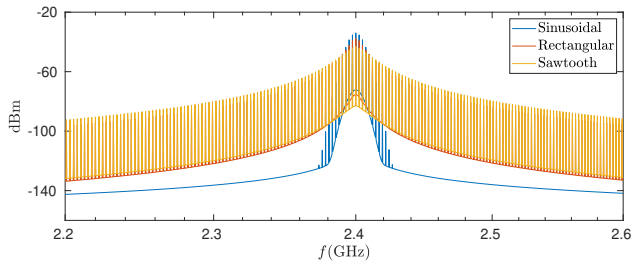

Fig. 4. Power displayed by an SA at the output of an SRO for each of the quench signals $k_a(t)$ in Fig. 3. RBW=100 kHz.

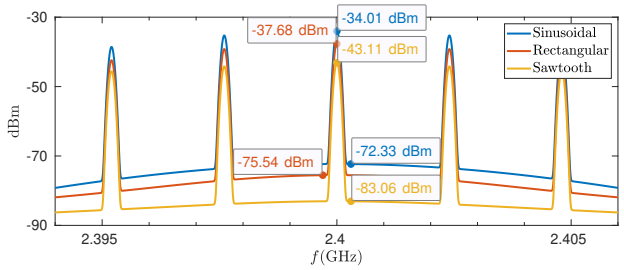

Fig. 5. Zoom in of Fig. 4. Power displayed by an SA at the output of an SRO for each of the quench signals $k_a(t)$ in Fig. 3. RBW=100 kHz.

they can be considered the same because the differences appear when the power levels are negligible compared to the maximum power. So, the relation between the PSD of noise and of the signal power spectrum can be considered constant for all frequencies, i.e.

$$\frac{P_{\text{signal SA}}(\omega_{0,n})}{P_{\text{noise SA}}(\omega_{0,n})} = \text{SNR}_{\text{raw}} \tag{20}$$

for all values of n. So, (19) becomes

$$\text{SNR}_{\text{SA}} = \text{SNR}_{\text{raw}} \frac{\text{ENBW}}{f_q}. \tag{21}$$

Even if the value SNR_{raw} could be evaluated at any frequency $\omega_{0,n}$, we will consider that this value is evaluated at ω_0. This way, the overall SNR is equal to the SNR in the interval $\Delta\omega_{0,0}$ as (17):

$$\text{SNR}_{\text{SA}} = \frac{P_{\text{signal SA}}(\omega_{0,0})}{P_{\text{noise SA}}(\omega_{0,0})} \frac{\text{ENBW}}{f_q}. \tag{22}$$

So, only two measurements are required to compute SNR. In the next section we explain how to experimentally do this measurements.

IV. Application Examples

Several simulations have been made to validate the fact that the overall SNR can be obtained from just two values displayed by the SA. We have used the *set of parameters* given in [17], with $f_0 = \frac{\omega_0}{2\pi} = 2.4\,\text{GHz}$ and $f_q = 2.4\,\text{MHz}$. For comparison, we take as a reference the *exact* SNR computed using (13). The literal use of (22) requires measuring separately the signal and the noise powers at the same frequency. Obviously this is not possible in practice because both sources overlap. We can solve this situation when the SRO is in the linear mode of operation by first measuring the output (due to noise) when no signal is applied at the input, and then measuring the output for signal levels high enough to make noise contribution negligible. Or, as an alternative also valid when the SRO is in the logarithmic mode of operation, we can measure the noise when signal is present by measuring the noise beside the signal peaks as is shown later in Fig. 5.

In Fig. 4 we can see the power displayed by an SA for a sinusoidal, rectangular and sawtooth quench signal with a RBW=100 kHz. The SNR computed using (13) is 24.757 dB for a sinusoidal quench, 24.338 dB for a rectangular quench and 26.301 dB for a sawtooth quench.

We can compare these reference values with the ones computed using (22). The RBW adjustment has been considered to be equal to the $\text{BW}_{3\text{ dB}}$. Using (2) and (3) we can compute ENBW from RBW as

$$\text{ENBW} = \frac{\sqrt{\pi}}{2\sqrt{\ln 2}}\text{RBW} \approx 1.0645\text{RBW}, \tag{23}$$

i.e., a 0.27 dB difference. We can express (22) in dB as

$$\text{SNR}_{\text{SA dB}} = P_{\text{signal SA}}(\omega_{0,0})_{\text{dBm}} - P_{\text{noise SA}}(\omega_{0,0})_{\text{dBm}} + 10\log_{10}\left(\frac{\text{ENBW}}{f_q}\right). \tag{24}$$

Figure 5 shows the signal power measurement made at the peak centered at f_0 and the noise power measurement made beside this peak. Using (24) we compute $\text{SNR}_{\text{SA dB}}$ for the sinusoidal quench signal as

$$\text{SNR}_{\text{SA dB}} = -34.01\,\text{dBm} + 72.33\,\text{dBm} + 10\log_{10}\left(\frac{\sqrt{\pi}\times 100\times 10^3}{2\times\sqrt{\ln 2}\times 2.4\times 10^6}\right) = 24.789\,\text{dB}, \tag{25}$$

value that is 0.032 dB greater than the reference (13). For the rectangular quench signal, (22) gives

$$\text{SNR}_{\text{SA dB}} = -37.68\,\text{dBm} + 75.54\,\text{dBm} + 10\log_{10}\left(\frac{\sqrt{\pi}\times 100\times 10^3}{2\times\sqrt{\ln 2}\times 2.4\times 10^6}\right) = 24.329\,\text{dB}, \tag{26}$$

value that is 0.009 dB lower than the reference (13), and for the sawtooth quench signal (22) gives

$$\text{SNR}_{\text{SA dB}} = -43.11\,\text{dBm} + 83.06\,\text{dBm} + 10\log_{10}\left(\frac{\sqrt{\pi}\times 100\times 10^3}{2\times\sqrt{\ln 2}\times 2.4\times 10^6}\right) = 26.419\,\text{dB}, \tag{27}$$

value that is 0.118 dB greater than the reference (13). We can conclude that the differences between (13) and (22) are negligible for practical purposes. Figure 6 shows the mesurements for a RBW= 50 kHz. As expected, halving the RBW decreases the noise power measurement by 3.01 dB, while the signal power measurement doesn't change. As a result the same $\text{SNR}_{\text{SA dB}}$ values are computed.

Note that the noise levels at the lower and upper limits of the frequency range shown in Fig. 4 are extremely low. In many circumstances, they will be masked by the noise floor of the SA, giving shapes such as the experimental results shown in Fig. 7-9 of the next section.

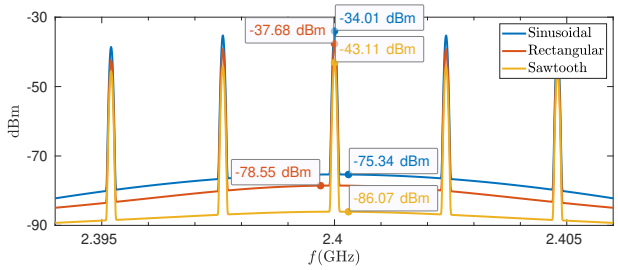

Fig. 6. Power displayed by an SA at the output of an SRO for each of the quench signals $k_a(t)$ in Fig. 3. RBW=50 kHz.

V. Laboratory Measurements

We have applied this technique in the laboratory to measure SNR at the output of an SRO tuned to work outside of the crowded 2.4 GHz band [20] with $f_0 = 2.584\,\text{GHz}$ and a sinusoidal quench with $f_q = 1\,\text{MHz}$. A Rohde & Schwarz SA was loosely coupled to an SRO by the usual procedure of building a small loop at the end of a coaxial cable and placing it near the SRO. In this way, there is no need to build a cumbersome probing system that might affect SR operation. Next we show the displayed results for different values of RBW that in this SA is equal to the $\text{BW}_{3\,\text{dB}}$. In Fig. 7 we can see (top right corner) that the difference between $P_{\text{signal SA}}(\omega_{0,0})_{\text{dBm}}$ and $P_{\text{noise SA}}(\omega_{0,0})_{\text{dBm}}$ is =16.12 dB. So, considering RBW=5 kHz, $f_q = 1\,\text{MHz}$, and (23) and (24):

$$\text{SNR}_{\text{SA dB}} = 16.12\,\text{dB} + 10\log_{10}\left(\frac{\sqrt{\pi}\times 5\times 10^3}{2\times\sqrt{\ln 2}\times 10^6}\right) = -6.62\,\text{dB}. \quad (28)$$

Using a RBW 10 times higher, i.e. RBW=50 kHz, will not change $P_{\text{signal SA}}(\omega_{0,0})_{\text{dBm}}$, while $P_{\text{noise SA}}(\omega_{0,0})_{\text{dBm}}$ will be increased 10 dB as is shown in Fig. 8, and as a consequence the computed SNR will be the same, i.e.

$$\text{SNR}_{\text{SA dB}} = 6.12\,\text{dB} + 10\log_{10}\left(\frac{\sqrt{\pi}\times 50\times 10^3}{2\times\sqrt{\ln 2}\times 10^6}\right) = -6.62\,\text{dB}. \quad (29)$$

Finally, doubling the RBW, i.e. RBW=100 kHz, will increase $P_{\text{noise SA}}(\omega_{0,0})_{\text{dBm}}$ by 3 dB as is shown in Fig. 9. Again, the computed SNR will be the same in practice.

VI. Conclusion

A simple and effective experimental method to quantify the SNR at which an SRO is operating has been presented. Exploiting the fact that the shape of the envelope of the signal power spectrum and the noise PSD is the same in the region where the power contribution is significant, we can determine the SNR by taking just two measurements of the power displayed by an SA. The relation between these two measurements is scaled by the RBW adjustment of the SA and the quench frequency of the SRO. Application examples for different RBW and quench signals have been provided.

The same method can be used to determine SNR in SROs operating in the logarithmic mode at a given signal input power. However, in this case the compression effect associated to this non-linear mode has the consequence that a 1 dB increase in the signal input power gives less than 1 dB increase in the signal output power and so, a decrease of the noise output power.

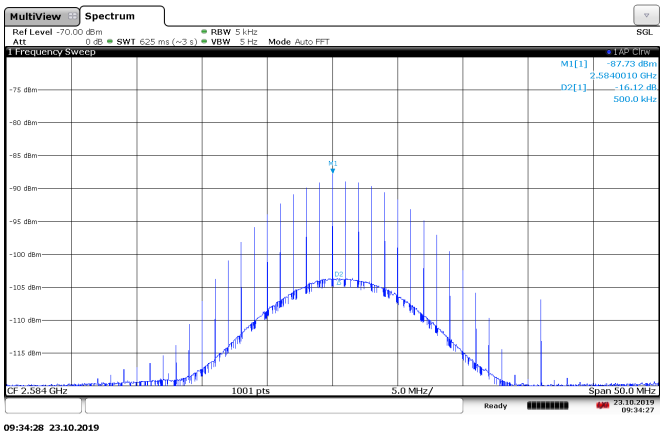

Fig. 7. Power displayed by an SA. RBW=5 kHz.

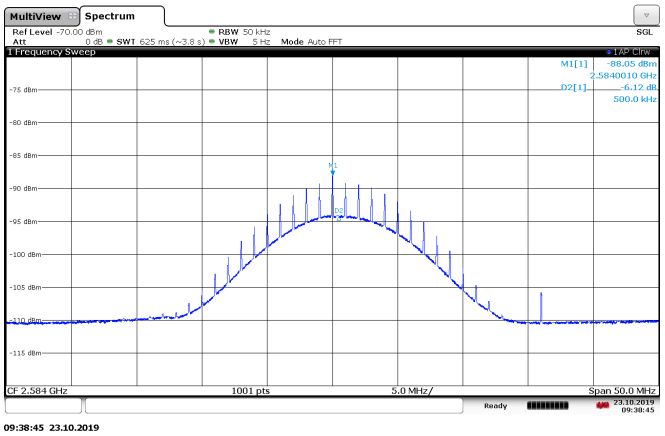

Fig. 8. Power displayed by an SA. RBW=50 kHz.

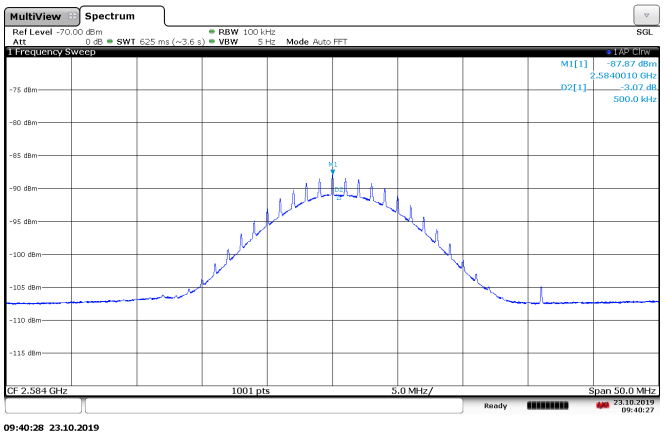

Fig. 9. Power displayed by an SA. RBW=100 kHz.

References

[1] E. Armstrong, "Some recent developments of regenerative circuits," *Proceedings of the Institute of Radio Engineers*, vol. 10, no. 4, pp. 244–260, Aug 1922.

[2] H. P. Kalmus, "Some notes on superregeneration with particular emphasis on its possibilities for frequency modulation," *Proceedings of the IRE*, vol. 32, no. 10, pp. 591–600, 1944.

[3] P. Pala-Schonwalder, J. Bonet-Dalmau, A. Lopez-Riera, F. Moncunill-Geniz, F. del Aguila-Lopez, and R. Giralt-Mas, "Superregenerative reception of narrowband FSK modulations," *Circuits and Systems I: Regular Papers, IEEE Transactions on*, vol. 62, no. 3, pp. 791–798, Mar 2015.

[4] L. Hernandez and S. Paton, "A superregenerative receiver for phase and frequency modulated carriers," in *Circuits and Systems, 2002. ISCAS 2002. IEEE International Symposium on*, vol. 3, 2002, pp. III–81–III–84 vol.3.

[5] P. Pala-Schonwalder, J. Bonet-Dalmau, F. Xavier Moncunill-Geniz, F. del Aguila-Lopez, and R. Giralt-Mas, "A superregenerative QPSK receiver," *Circuits and Systems I: Regular Papers, IEEE Transactions on*, vol. 61, no. 1, pp. 258–265, Jan 2014.

[6] M. Pelissier, D. Morche, and P. Vincent, "Super-regenerative architecture for UWB pulse detection: From theory to RF front-end design," *IEEE Transactions on Circuits and Systems I: Regular Papers*, vol. 56, no. 7, pp. 1500–1512, July 2009.

[7] B. Zhou and P. Chiang, "Short-range low-data-rate fm-uwb transceivers: Overview, analysis, and design," *IEEE Transactions on Circuits and Systems I: Regular Papers*, vol. 63, no. 3, pp. 423–435, March 2016.

[8] A. López-Riera, F. del Águila López, P. Palá-Schönwälder, J. Bonet-Dalmau, R. Giralt-Mas, and F. X. Moncunill-Geniz, "Joint symbol and chip synchronization for a burst-mode-communication superregenerative MSK receiver," *IEEE Transactions on Circuits and Systems I: Regular Papers*, vol. 64, no. 5, pp. 1260–1269, May 2017.

[9] M. Anis, M. Ortmanns, and N. Wehn, "A 2.5mw 2mb/s fully integrated impulse-FM-UWB transceiver in 0.18 μm CMOS," in *2011 IEEE MTT-S International Microwave Symposium*, June 2011, pp. 1–3.

[10] R. Rieger and N. Sulistiyanto, "Integrated circuit for super-regenerative low-frequency amplification," *IEEE Transactions on Circuits and Systems II: Express Briefs*, vol. 65, no. 1, pp. 31–35, Jan 2018.

[11] H. Fuketa, S. O'uchi, and T. Matsukawa, "A 0.3-V 1-μW super-regenerative ultrasound wake-up receiver with power scalability," *IEEE Transactions on Circuits and Systems II: Express Briefs*, vol. 64, no. 9, pp. 1027–1031, Sept 2017.

[12] F. Moncunill-Geniz and P. Pala-Schonwalder, "Performance of a DSSS superregenerative receiver in the presence of noise and interference," in *Circuits and Systems, 2006. ISCAS 2006. Proceedings. 2006 IEEE International Symposium on*, May 2006, pp. 5687–5690.

[13] P. Thoppay, C. Dehollaini, and M. Declercq, "Noise analysis in super-regenerative receiver systems," in *Research in Microelectronics and Electronics, 2008. PRIME 2008. Ph.D.*, Jun 2008, pp. 189–192.

[14] D. G. Lee and P. P. Mercier, "Noise analysis of phase-demodulating receivers employing super-regenerative amplification," *IEEE Transactions on Microwave Theory and Techniques*, vol. 65, no. 9, pp. 3299–3311, Sept 2017.

[15] J. Bohorquez, A. Chandrakasan, and J. Dawson, "Frequency-domain analysis of super-regenerative amplifiers," *Microwave Theory and Techniques, IEEE Transactions on*, vol. 57, no. 12, pp. 2882–2894, Dec 2009.

[16] S. Sancho, S. Hernández, and A. Suárez, "Noise analysis of super-regenerative oscillators in linear and nonlinear modes," *IEEE Transactions on Microwave Theory and Techniques*, vol. 67, no. 12, pp. 4955–4965, 2019.

[17] J. Bonet-Dalmau, P. Palà-Schönwälder, F. X. Moncunill-Geniz, F. del Águila-López, and R. Giralt-Mas, "Signal and noise power spectra in superregenerative oscillators," in *2019 IEEE International Symposium on Circuits and Systems (ISCAS)*, May 2019, pp. 1–5.

[18] J. Bonet-Dalmau, F. Moncunill-Geniz, P. Pala-Schonwalder, F. del Aguila-Lopez, and R. Giralt-Mas, "Frequency domain analysis of super-regenerative receivers in the linear and the logarithmic modes," *Circuits and Systems I: Regular Papers, IEEE Transactions on*, vol. 59, no. 5, pp. 1074–1084, May 2012.

[19] P. Palà-Schönwälder, J. Bonet-Dalmau, F. del Águila López, R. Sanahuja, and F. X. Moncunill-Geniz, "Effects of quench discretization on superregenerative oscillators," in *2012 IEEE International Symposium on Circuits and Systems*, May 2012, pp. 1303–1306.

[20] F. X. Moncunill-Geniz, C. Dehollain, N. Joehl, M. Declercq, and P. Pala-Schonwalder, "A 2.4-ghz low-power superregenerative rf front-end for high data rate applications," in *2006 European Microwave Conference*, Sep. 2006, pp. 1537–1540.